Critical role of polymer-ceramic ion exchange for high conductivity composite electrolytes

Amit Bhattacharya^{a, #}, Ji-young Ock^{b, #}, Tao Wang^b, James T. Bamford^c, Rachel A. Segalman^c
Sheng Dai^b, Alexei P. Sokolov^{b, *}, Xi Chelsea Chen^{b, *}, Raphaële J. Clément^{a, *}
(#A.B. and J.O. equally contributed to this work.)

^a Materials Department and Materials Research Laboratory, University of California, Santa Barbara, California, 93106, United States

^b Chemical Sciences Division, Oak Ridge National Laboratory, 1 Bethel Valley Road, Oak Ridge, TN, 37830, United States

^c Materials Department and Department of Chemical Engineering, University of California, Santa Barbara, California 93106, United States

This manuscript has been authored by UT-Battelle, LLC, under contract DE-AC05-00OR22725 with the U.S. Department of Energy. The United States government retains and the publisher, by accepting the article for publication, acknowledges that the United States government retains a nonexclusive, paid-up, irrevocable, world-wide license to publish or reproduce the published form of this manuscript or allow others to do so for United States government purposes. The Department of Energy will provide public access to these results of federally sponsored research in accordance with the DOE Public Access Plan (http://energy.gov/downloads/doepublic-access-plan).

ABSTRACT

Polymer-ceramic composites offer a path to enhance the transport and mechanical properties of solid electrolytes. However, an in-depth understanding of the extent and role of ion transport along and across polymer-ceramic interfaces in these systems is lacking. We have recently shown that Li-conducting Li_{0.11}Na_{0.24}K_{0.02}La_{0.43}TiO_{2.82} (LMTO) nanorods can be prepared by a molten flux method, and the addition of 30-50 weight (wt.)% LMTO to a bis[(trifluoromethyl)sulfonyl]imidevinyl ethylene carbonate-based single-ion conducting (SIC) polymer electrolyte leads to a twofold enhancement in Li-ion conductivity, from 1.4 to 3.0×10^{-5} S/cm at 30 °C. In the present study, we use NMR methods to identify the Li-ion transport pathways and determine the timescale of chemical exchange between the SIC polymer and LMTO ceramic components. Tracer exchange NMR indicates preferential transport through the polymer or polymer-interfacial regions, and exchange spectroscopy (EXSY) and a new isotope exchange method reveal negligible Li exchange between the SIC polymer and LMTO ceramic up to several days. Here, LMTO nanorods act as a passive filler. Our results further highlight that significant (e.g., 10- or 100-fold) conductivity enhancements in composite electrolytes can only be achieved 1) with ionically-conductive fillers, and 2) when both the ceramic and polymer components actively participate in long-range transport. For this, fast interfacial ion exchange is needed. This leads us to introduce a critical interfacial ion exchange time to evaluate whether a filler actively contributes to conduction in a composite electrolyte, and screen for promising polymer-ceramic pairings to accelerate the development of high conductivity solid electrolytes.

Keywords

Battery Solid electrolyte, Polymer, Ceramic, NMR, Ion transport, Tracer exchange

1. Introduction

Solid-state batteries (SSBs) are increasingly recognized as a transformative energy storage technology, holding promise in terms of safety and energy density compared to traditional lithium (Li)-ion cells containing a liquid electrolyte. Unfortunately, the large-scale implementation of SSBs is still impeded by challenges regarding the design of solid electrolytes and solid-solid interfaces for long-lasting performance [1–7]. An ideal solid electrolyte exhibits high ionic conductivity, a moderate bulk modulus or high toughness to accommodate the volume changes at the electrodes during electrochemical cycling and maintain a stable solid electrolyte interphase (SEI), strong adhesion to electrodes, good processability, and a wide electrochemical stability window [8]. Polymer electrolytes, while flexible and easy to process, often fall short in terms of conductivity, limiting their performance [9–11]. The more widely used polymer electrolyte, poly(ethylene oxide) (PEO), requires the device to be operated at ~90 °C, where its ionic conductivity is on the order of 10⁻³ to 10⁻⁴ S/cm [12]. Its performance drops precipitously at around 65 °C, where PEO chains start to crystallize [13], and its poor room temperature ionic conductivity, on the order of 10⁻⁶ to 10⁻⁵ S/cm, cannot compete with that of organic-based liquid electrolytes (10⁻³ to 10⁻² S/cm) [14]. Ceramic electrolytes exhibit a range of ionic conductivities and electrochemical stabilities, depending on the chemistry [15-19], but invariably suffer from insufficient ductility and poor electrode adhesion [20,21], despite the use of energy-intensive hot sintering/pressing protocols and high stack pressures to improve contacts between the solid components during device fabrication [22,23].

Several strategies have been employed to develop polymer electrolytes that combine good mechanical strength with a high ionic conductivity [24]. For example, the use of a polystyrene (PS)-PEO block copolymer has been proposed, in which the PS block provides mechanical strength, and the oligomeric (low-molecular weight) PEO block provides ionic conductivity at elevated temperature [25,26]. Other studies have relied on nanostructuring via polymerization-induced phase separation [27], the formation of crosslinked nanoparticle-polymer composites [28], dynamic network polymers, such as through metal-ligand coordination [29] or domain-limited ion transport [30]. Additionally, the incorporation of inorganic fillers into the polymer matrix has been shown to enhance ionic transport and improve mechanical integrity [31–35]. Inorganic fillers are categorized as passive (e.g., SiO₂, TiO₂) or active (e.g., Li₃N, LiAlO₂); passive fillers exhibit a

relatively low ionic conductivity (<10⁻⁴ S/cm) whereas active fillers show a higher ionic conductivity than the polymer electrolyte at typical operating temperatures. In such composite electrolytes, ionic conductivity enhancements have been attributed to the formation of polymer-ceramic interfaces enabling fast ion transport, or to polymer plasticization, whereby the filler particles act as solid plasticizers that kinetically inhibit polymer crystallization, or to the establishment of a percolating network of conductive particles (for active fillers) [36,37].

A major challenge in designing hybrid electrolytes is the lack of a clear understanding of the extent and role of ion transport along and across the polymer-ceramic interface, due to the dearth of methodologies that can directly probe ion conduction pathways [38–40]. Li-ions can move through the polymer phase, the ceramic phase, and in the interfacial region. Chemical exchange of Li species also takes place between the bulk polymer and ceramic components. In fact, when an active filler is used with a higher bulk ionic conductivity than the polymer matrix, Li-ion transport still crucially depends on chemical exchange between the ceramic and polymer phases, *i.e.*, across the interface.

The present work builds upon two recent studies [41,42] of hybrid electrolytes comprising perovskite inorganic fillers in a TFSI-vinyl ethylene carbonate (VEC) based single-ion conducting (SIC) polymer matrix. We focus on perovskite-type lithium lanthanum titanate (LLTO) ceramics due to their high conductivity, up to 4.0 x 10⁻³ S/cm at room temperature for single-crystalline La_{0.5}Li_{0.5}TiO₃ (LLTO) [43], and our ability to produce A-site disordered cubic perovskite $La_{0.5}M_{0.5}TiO_3$ (LMTO, M = Li, Na, K) single-crystalline nanorods using a NaCl-KCl molten flux method and commercial P25-TiO₂ precursor nanoparticles, as described in our previous work [42]. The stabilization of the cubic form of LLTO is beneficial for bulk ion transport, while the formation of single-crystal nanorods eliminates issues of sluggish Li-ion transport across grain boundaries that have plagued polycrystalline LLTO electrolytes [44], and maximizes the interface-to-ceramic volume ratio in the composite. Comparing the ionic conductivity and Li diffusivity of hybrid perovskite-SIC electrolytes comprising 50 wt.% of either micron-sized LLTO or our LMTO nanorods prepared using the flux method, we found that the addition of LMTO nanorods leads to a two-fold enhancement in the room temperature ionic conductivity compared to the neat SIC polymer, from 1.4 to 3.0×10^{-5} S/cm, while the addition of bulk LLTO has a negligible impact on ion transport. These results suggest that the Li-ion transport properties depend primarily on the perovskite particle size and morphology, and potentially their surface chemistry [41,42]. Further, the temperature-dependent conductivity of the SIC-LMTO composite showed Vogel-Fulcher-Tammann (VFT) behavior, indicating that Li-ions primarily move through the polymer matrix despite the low activation energy barrier (ca. 0.3 eV) for Li-ion transport within the LMTO phase determined from nuclear magnetic resonance (NMR) spectroscopy. Finally, conductivity data obtained on a series of SIC-based composite electrolytes with LMTO nanorod loadings varying from 10 to 50 wt.% suggested that the interfacial polymer layers percolate through the composite around 30 wt. % (9.5 vol %). Overall, these findings reveal that the Li-ion conductivity enhancements observed in SIC-LMTO composites stem from the formation of a percolating network of polymer-ceramic interfacial regions. However, direct experimental evidence for rapid interfacial Li-ion transport and an understanding of the role of the ceramic particles in the SIC-LMTO composite is still lacking.

NMR spectroscopy is among the very few techniques that can provide information about the local environments and dynamics of Li-ions in complex systems comprising multiple phases and/or amorphous components. In recent years, $^6\text{Li}\rightarrow ^7\text{Li}$ tracer exchange NMR spectroscopy has emerged as an attractive approach for probing Li-ion transport pathways within composite electrolytes [45–49]. This technique involves passing a constant current across a Li/Li symmetric cell comprising a natural abundance hybrid electrolyte (i.e., 7.6% ⁶Li and 92.4% ⁷Li [50]) sandwiched between two ⁶Li-enriched metallic electrodes. As a result, the isotopic content of the electrolyte evolves over the course of electrochemical cycling, with ⁷Li being replaced by ⁶Li along the preferred Li-ion conduction pathways. Such pathways can readily be identified by monitoring the change in the relative intensity of the ⁶Li NMR signals attributed to the ceramic, polymer, and interfacial components of the electrolyte. Tracer exchange experiments have so far exclusively been conducted on ex situ electrolyte samples harvested from electrochemical cells and analyzed after the current has stopped. Hence, the accuracy of the method relies on ultraslow chemical exchange between the polymer, interface, and ceramic, such that ⁶Li enrichment of the more conductive region(s) is retained hours or even days after the electrolyte sample has been extracted from the cell. We illustrate the two possible scenarios of ultraslow and faster chemical exchange in Figure 1, in the ideal case where the polymer, ceramic and interfacial signals are well resolved. In scenario 1 where Li chemical exchange between the various regions is extremely slow (> hours or days) and Li-ions preferentially transport through the polymer/ceramic interfacial region rather than in the bulk polymer or ceramic regions, the ⁶Li resonance corresponding to the interface is enhanced.

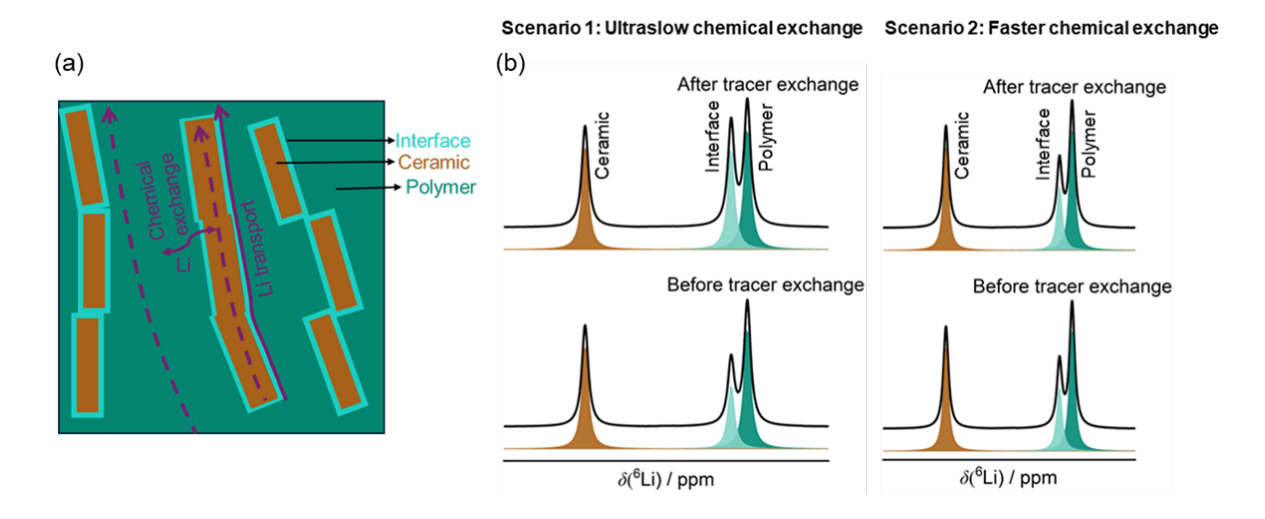


Figure 1. (a) Schematic of Li transport pathways and (b) illustration of possible outcomes of ${}^6\text{Li} \rightarrow {}^7\text{Li}$ tracer exchange NMR experiments on hybrid polymer electrolytes exhibiting ultraslow (scenario 1) and faster (scenario 2) Li chemical exchange between the polymer, ceramic, and interfacial regions. In scenario 1, an enhancement in the interfacial ${}^6\text{Li}$ signal is observed, whereas in scenario 2, no change is noted.

In scenario 2, however, Li chemical exchange between the different regions occurs on a faster timescale (this could still be on the order of seconds), and no signal enhancement is expected due to re-equilibration of the ⁶Li/⁷Li populations in the various regions of the electrolyte, precluding the assessment of Li-ion transport pathways.

Further complications arise when the rate of Li exchange between the ceramic and/or polymer and the interface is on the order of the frequency difference (typically, 100s-1000s Hz) between the corresponding ^{6/7}Li NMR resonances, resulting in signal averaging and making it difficult to differentiate the contributions from the different regions [51]. Two-dimensional exchange spectroscopy (2D EXSY) NMR is a powerful approach to probe the kinetics of Li chemical exchange on the millisecond to second timescale but cannot be used to study extremely slow exchange processes on the order of minutes to days.

Here, we combine ⁶Li→⁷Li tracer exchange spectroscopy, 2D EXSY, as well as a new isotope exchange NMR method capable of probing very slow chemical exchange up to hours/days, to identify the Li-ion transport pathways and determine the timescale of chemical exchange between the various regions of the SIC-LMTO hybrid electrolyte. The tracer exchange experiments reveal

preferential Li-ion transport through the polymer interfacial regions. The EXSY and long-term isotope exchange experiments indicate no Li exchange between the polymer and ceramic regions of the composite on the second timescale, as evidenced by the absence of cross-peaks in the 2D EXSY spectrum up to 3 seconds of mixing time, and on the timescale of days, respectively, even at 80 °C. These results indicate that Li exchange between the SIC and LMTO components falls within the "ultraslow" exchange regime such that the LMTO nanorods act as a passive filler and likely enhance conductivity by reducing electrostatic interactions between Li-ions and the polyanion matrix. Overall, these findings highlight the fundamental limitations of passive fillers, which we suggest can only provide marginal improvements in the transport properties of a polymer matrix. While active fillers are essential to the development of high conductivity electrolytes, the establishment of long-range conduction pathways through both the ceramic and polymer regions also requires fast interfacial ion exchange. In the last section of this paper, we therefore introduce a new criterion, the critical interfacial ion exchange time, which allows to determine whether ceramic particles actively contribute to long-range ion transport in a composite electrolyte.

2. Experimental

2.1. Materials and ceramic synthesis

P25-TiO₂ (30-40 nm) was purchased from Nanostructured & Amorphous Materials Inc. LiNO₃, La(NO₃)·6H₂O were purchased from Sigma-Aldrich. KCl and NaCl were purchased from Fisher. All chemicals were used as received. Vinyl ethylene carbonate (VEC, Sigma-Aldrich) was dried over molecular sieves and stored in an Ar-filled glovebox before use. Both lithium sulfonyl(trifluoromethane sulfonyl)imide styrene (LiSTFSI, SPECIFIC POLYMERS) and lithium sulfonyl(trifluoromethane sulfonyl)imide methacrylate (LiMTFSI, SPECIFIC POLYMERS) were kept in the glovebox and used as received. Recrystallized Azobisisobutyronitrile (AIBN, Sigma-Aldrich) was also stored in the glovebox. Polyethylene glycol dimethacrylate (PEGDMA, Polysciences) was kept in the glovebox and used as received.

The synthesis of Li_{0.11}Na_{0.24}K_{0.02}La_{0.43}TiO_{2.82} (LMTO) nanorods was described in our previous work [41,42]. P25-TiO₂, LiNO₃, La(NO₃)₃·6H₂O, KCl, and NaCl precursors were combined in a mass ratio of 1:2:0.3:2.8:2.2. The components were thoroughly mixed in an agate mortar,

subsequently ball-milled for 5 minutes in a ZrO₂ jar and dried at 473 K for 2 hours in an oven. Then, the dried mixture was heated to 1073 K at a ramp rate of 5 K/min and held at 1073 K for 5 hours in an alumina crucible under air. After naturally cooling to room temperature, the residual salts were removed via vacuum filtration with water. The resulting white solid was dried at 383 K for 2 hours in a vacuum oven, ground into a fine powder using an agate mortar, and then subjected to a final heat treatment at 873 K for 2 hours at a ramp rate of 5 K/min in air to yield the LMTO nanorods. ⁶Li-LMTO nanorods were synthesized using a similar procedure, but combining P25-TiO₂, ⁶LiOH, La(NO₃)₃·6H₂O, KCl, and NaCl in a mass ratio of 1:0.7:0.3:2.8:2.2.

2.2. Synthesis of buffer polymer electrolytes and composite electrolytes

The synthesis details have been reported elsewhere [37, 38]. Briefly, for the preparation of the buffer polymer, VEC, LiSTFSI, PEGDMA, and AIBN were combined in a glass vial and stirred in an Ar glovebox until dissolved. The weight ratio of VEC to PEGDMA was fixed at 7:3. The solution was cast between two glass plates with mylar membrane, separated by cover glass slips, and cured at 80 °C on a hot plate for 1 hour. The resulting free-standing buffer polymer was punched into 5/8" discs and stored in an Ar-filled glovebox without further drying. To prepare the SIC-30wt.% LMTO composite electrolytes, VEC, LiMTFSI, AIBN, LMTO nanorods and yttria-stabilized zirconia milling balls were combined inside a polypropylene vial inside the glovebox. Subsequently, the vial was tightly sealed, wrapped with Parafilm, and transferred outside the glovebox for thorough mixing using a Turbula Mixer (GlenMills INC.) for 10 minutes. The blended mixture was subsequently returned to the glovebox to seal in an airtight mason jar, and the polymerization was then performed overnight in a thermostat chamber (Heratherm OGH60, Thermo SCIENTIFIC) at 80 °C.

2.3. Preparation of ${}^6Li \rightarrow {}^7Li$ tracer exchange samples and electrochemical testing

To prepare composite electrolyte samples for ${}^{6}\text{Li} \rightarrow {}^{7}\text{Li}$ tracer exchange measurements, we assembled 2032-type coin cells in an Ar-filled glovebox. To prepare ⁶Li metal disc electrodes, the surface of ⁶Li metal chunks (Cambridge Isotope, 95%) was carefully shaved off before flattening the pieces using a roll and punching 7/16" discs. The mask used to contain the composite electrolyte within the battery stack and ensure a thickness of ~1 mm was assembled by stacking 10 Mylar washers (outer diameter: 5/8", inner diameter: 7/16") and gluing them together. To assemble the coin cell, a buffer polymer membrane was placed on top of the bottom ⁶Li disc electrode, followed by the Mylar mask, which was subsequently filled with the polymerized composite electrolyte. Then, another buffer polymer membrane was stacked on top of the composite layer, followed by the top ⁶Li disc electrode (Figure 2a). Galvanostatic cycling and electrochemical impedance spectroscopy (EIS) measurements were conducted using a VSP-3e Biologic potentiostat. All cells were conditioned at 70 °C for at least 12 hours before cell testing, which was also conducted at 70°C using a thermostat chamber (SU-222, ESPEC). Galvanostatic cycling was conducted using cut-off potentials of -5 V and +5 V vs. Li/Li⁺ at a current density of 0.048 mA/cm² and at an areal capacity of 0.012 mAh/cm². The cell impedance at open circuit potential was measured before and after cycling in the frequency range from 1 MHz to 100 mHz with a voltage amplitude of 6 mV. The cells were disassembled post cycling inside the glovebox and the cycled composite electrolyte samples were scraped off for ⁶Li→⁷Li tracer exchange analysis.

2.4. NMR spectroscopy

All solid-state one-dimensional $^{6/7}$ Li and two-dimensional (2D) 6 Li EXSY NMR spectra were collected at 18.8 T on a Bruker AVANCE standard bore III Ultrashield Plus spectrometer using a 2.5 mm H-X magic angle spinning (MAS) probe. All samples were packed into 2.5 mm (O.D.) zirconia rotors inside the Ar-filled glovebox and spun at 30 kHz during NMR measurements. 1D 6 Li data on SIC-30wt.%LMTO were acquired with a $\pi/2$ pulse of 4 μ s at 200 W with recycle delay of 60-80 s. 1D 7 Li NMR experiments were performed on SIC-30wt.%LMTO and SIC-50wt.% LMTO using $\pi/6$ pulse of 0.56 μ s at 200 W with recycle delay 10 s at 30 $^\circ$ C and 80 $^\circ$ C. 6 Li- 6 Li 2D EXSY experiments for SIC-50wt.% LMTO were acquired using a standard three-pulse sequence

with $\pi/2$ pulse of 4 μ s, mixing times of 0 –3 s and a relaxation delay of 60 s at 60 and 80 °C. 16 scans were collected for each of the 80-160 data points in indirect dimension. A nitrogen gas flow at a rate of 2000 L/h was employed to regulate the rotor temperature and protect the sample from moisture. All ^{6/7}Li spectra were referenced to an aqueous lithium chloride solution (1 M LiCl, δ_{iso} = 0 ppm). NMR spectra were processed using the Bruker TOPSPIN 4.4.0, fitted and plotted using Origin2024 software package.

3. Results and discussion

In this study, vinyl ethylene carbonate (VEC) was combined with lithium sulfonyl (trifluoromethane sulfonyl)imide methacrylate (MTFSILi) to form a copolymer. This copolymerization process yielded a single-ion-conducting (SIC) polymer electrolyte composed of 99% polymerized MTFSILi polyanion segments and approximately 44% polymerized VEC segments. Li_{0.11}Na_{0.24}K_{0.02}La_{0.43}TiO_{2.82} (LMTO) nanorods with an average diameter of ~33 nm and a length of ~150 nm were used as inorganic filler to prepare SIC-30wt.% LMTO and SIC-50wt.% LMTO hybrid electrolytes through a one-pot synthesis method. Details of the synthesis and basic characterization of the SIC and LMTO components, and of the SIC-LMTO blend, were reported in our recent work [41,42].

Previously, we showed that the LMTO nanorods are conductive to Li, with an activation energy barrier on the order of 0.3 eV obtained from variable-temperature NMR [42]. We also recorded an increase in the room temperature ionic conductivity from 1.4 × 10⁻⁵ S/cm for pure SIC to 3.0 × 10⁻⁵ S/cm for an SIC-50wt.% LMTO composite electrolyte, while the addition of a similar amount (50 wt.%) of commercial, micron-sized La_{0.5}Li_{0.5}TiO₃ (LLTO) particles to the polymer matrix led to no such improvement [41,42]. A gradual increase in the total ionic conductivity of composite SIC-LMTO electrolytes was observed upon increasing the weight fraction of nanorods up to 30 wt.%, followed by a saturation at higher ceramic loadings. This result was explained by the formation of a percolating network of Li-conductive interfacial regions at and above 30 wt.% ceramic loading [41]. However, our previous work did not provide direct evidence for preferential interfacial Li-ion transport in SIC-LMTO composites, and it remains unclear whether LMTO particles actively contribute to the measured conductivity.

To identify the preferred Li-ion transport pathway within the SIC-LMTO composite, a symmetric tracer exchange cell with composition [⁶Li|buffer polymer|SIC-30 wt.% LMTO composite|buffer polymer|⁶Li] was assembled in an Ar-filled glovebox (**Figure 2a**). Here, the electrodes consist of pure ⁶Li metal and the composite electrolyte contains natural abundance Li (*i.e.*, 7.6% ⁶Li and 92.4% ⁷Li). As Ti⁴⁺ species in LMTO can be reduced upon contact with Li metal [22], we incorporated an electrochemically-stable [52] buffer polymer layer between the electrolyte of interest and the electrodes to mitigate degradation [53]. This buffer polymer is a crosslinked membrane consisting of VEC and lithium sulfonyl(trifluoromethane sulfonyl)imide styrene (LiSTFSI), with a corresponding ⁶Li NMR resonant frequency that is conveniently distinct from that of our hybrid electrolyte, resulting in adequate spectral resolution for the tracer exchange study.

We first examined the electrochemical properties of the [⁶Li|buffer polymer|SIC-30 wt.% LMTO composite|buffer polymer|⁶Li] symmetric cell. The cell was conditioned at 70 °C for 12 hrs before undergoing 30 charge-discharge cycles at a constant current density of 0.048 mA/cm² and using cut-off potentials of –5 V and +5 V vs. Li/Li⁺. The resulting charge-discharge profiles are shown in **Figure 2b** and reveal no cell short up to cycle 30. A cumulative total capacity (sum of the total plating and stripping capacities) of 0.72 mAh/cm² was passed through the cell over the course of the measurement, corresponding to roughly 3.6 μm of Li/cm² or 0.026 mmol of Li, *i.e.*, approximately 23% the total amount of Li in the composite electrolyte and buffer polymer layers (around 0.113 mmol). The amount of ⁶Li passed through the cell over the 30 cycles sets an upper bound to the amount of ⁶Li that can be enriched in the composite electrolyte layer harvested after cycling, as some of the ⁶Li will remain in the buffer polymer layers or may plate onto the metallic electrodes.

The electrochemical performance of the [6Li|buffer polymer|SIC-30 wt.% LMTO composite|buffer polymer|6Li] symmetric cell is compared to that of a cell comprising a single buffer polymer layer sandwiched between the two 6Li metal electrodes in **Figure S1a**. These two symmetric cells were also analyzed using electrochemical impedance spectroscopy (EIS) to monitor the evolution of their bulk and interfacial resistances before and after cycling (**Figures S1b** and **S1c**). The depressed semicircle in the high frequency region (> 19 kHz) is attributed to the bulk polymer resistance, and the second semicircle in the mid to low frequency region (< 19

kHz) is mainly attributed to the buffer polymer/Li metal interfacial resistance and is consistent with a previous report [52]. As expected, the cell comprising the thick buffer polymer|composite|buffer polymer sandwich shows a larger bulk resistance than the single-layer cell, consistent with its slightly higher overpotential (**Figure S1a**). The cells' bulk resistances do not evolve significantly upon cycling but their interfacial resistances increase from 96 to 484 ohms for the composite electrolyte cell, and from 509 to 670 ohms for the single-layer cell, after 30 cycles (**Table S1**), presumably due to (an) electrochemical reaction(s) or loss of contact between the buffer polymer and the electrodes. The stability of the polymer|Li metal interface is affected by the Li₂CO₃, Li₂O and LiOH phases present at the surface of metallic Li, its surface roughness, and microstructure [54]. Here, we shaved off the surface of the ⁶Li metal chunks used to prepared the disc electrodes, eliminating the native passivation layer, which may have reduced the interfacial stability. Overall, the electrochemical testing and EIS results indicate that the [⁶Li|buffer polymer|SIC-30 wt.% LMTO composite|buffer polymer|⁶Li] cell shows sufficiently good cycling stability and that enough Li is exchanged over the course of the measurement for the resulting composite electrolyte samples to be used for tracer exchange experiments.

The room temperature 'Li solid-state NMR spectrum collected on the SIC-30 wt.% LMTO composite electrolyte extracted from a cell conditioned at 70 °C for 12 h (no electrochemical cycling) exhibits four distinct resonances (Figure 2c). The signal at -1.5 ppm is assigned to residual buffer polymer (peak #), the signal at -1.1 ppm is attributed to the SIC polymer (peak 1), the signal at -0.5 ppm is assigned to the LMTO ceramic (peak 2), and the signal at -0.07 ppm to a minor decomposition product (peak 3). We note that the signals from the bulk polymer region and polymer interfacial region cannot be distinguished in our measurements and fall under peak 1 at -1.1 ppm; this could either be due to significant signal overlap or, more likely, to fast Li-ion exchange between the bulk and interfacial polymer regions, leading to an average polymer signal. Indeed, if the rate of exchange (k_{ex}) between Li environments in the bulk and interfacial polymer regions fulfills the condition $k_{ex} \approx \pi \Delta v / \sqrt{2}$, where Δv is the difference in resonant frequency (in Hz) between the two Li environments, the individual signals will coalesce into one broad signal that will sharpen as k_{ex} increases. Assuming that the NMR resonances from Li species in the bulk and interfacial polymer regions are separated by 0.5 ppm, then $\Delta \nu \approx$ 59 Hz at 18.8 T, and k_{ex} should be \geq 131 Hz for the signals to coalesce. We can estimate k_{ex} from our previous work, where we determined that the thickness of the interfacial polymer region was on the order of $L\sim 5$ nm, and measured an average room temperature ⁷Li self-diffusion coefficient $D = 1.3 \times 10^{-12} \, m^2/s$ for transport within the polymer matrix by pulsed field gradient (PFG) NMR [41]. Using these two parameters, the diffusion time (τ) through the polymer interfacial region can be estimated using the Einstein-Smoluchowski relation in three dimensions, $\langle r^2 \rangle = 6D\tau$, where $\langle r^2 \rangle$ is the mean square displacement. This leads to a diffusion time $\tau = \frac{L^2}{6D} \approx 3.2 \times 10^{-6} s$, hence an exchange rate k_{ex} in the MHz range, confirming that the single SIC polymer resonance arises from signal averaging due to rapid Li chemical exchange between the bulk and interfacial polymer regions. The decomposition product presumably forms during the conditioning step as it is not present in the spectrum obtained before conditioning. To gain further insights into possible decomposition reactions at the buffer polymer|Li metal interface during conditioning and cycling, a 6Li NMR spectrum was collected on a buffer polymer sample extracted from a single-layer cell after 30 cycles and is compared to the spectrum obtained on a pristine buffer polymer sample in Figure S2. The two spectra are very similar and no additional, broad resonance is observed in the data collected after cycling, which indicates that 1) the decomposition product leading to peak 3 presumably arises from slight degradation of the composite electrolyte during cell conditioning, which does not significantly impact cell cycling, and 2) potential electrochemical reactions at the buffer polymer|Li metal interface (discussed in the previous paragraph) are likely minor as they do not lead to any detectable degradation product.

The room temperature 6 Li solid-state NMR spectrum collected on a SIC-30wt.% LMTO sample extracted after 30 electrochemical cycles exhibits the same resonances as those observed for the sample obtained post conditioning (**Figure 2c**), minus the buffer polymer resonance as this layer was successfully removed prior to analysis. The fraction of 6 Li integrated signal intensity corresponding to the SIC polymer relative to the total integrated signal intensity arising from the hybrid electrolyte layer [peak 1/ (peak 1+ peak 2+ peak 3)] increases from 72 ± 2 % before cycling to 80 ± 2 % after cycling (**Table S2**), indicating preferential Li-ion conduction through the SIC polymer or in the polymer interfacial region. This result is corroborated by the 7 Li NMR data collected on the same *ex situ* samples shown in **Figure S3**, where the fraction of 7 Li integrated signal intensity corresponding to the SIC resonance [peak 1/ (peak 1+ peak 2+ peak 3)] decreases from 38 ± 4 % before cycling to 28 ± 2 % after cycling, implying a depletion of the 7 Li nuclei in the polymer or interfacial regions.

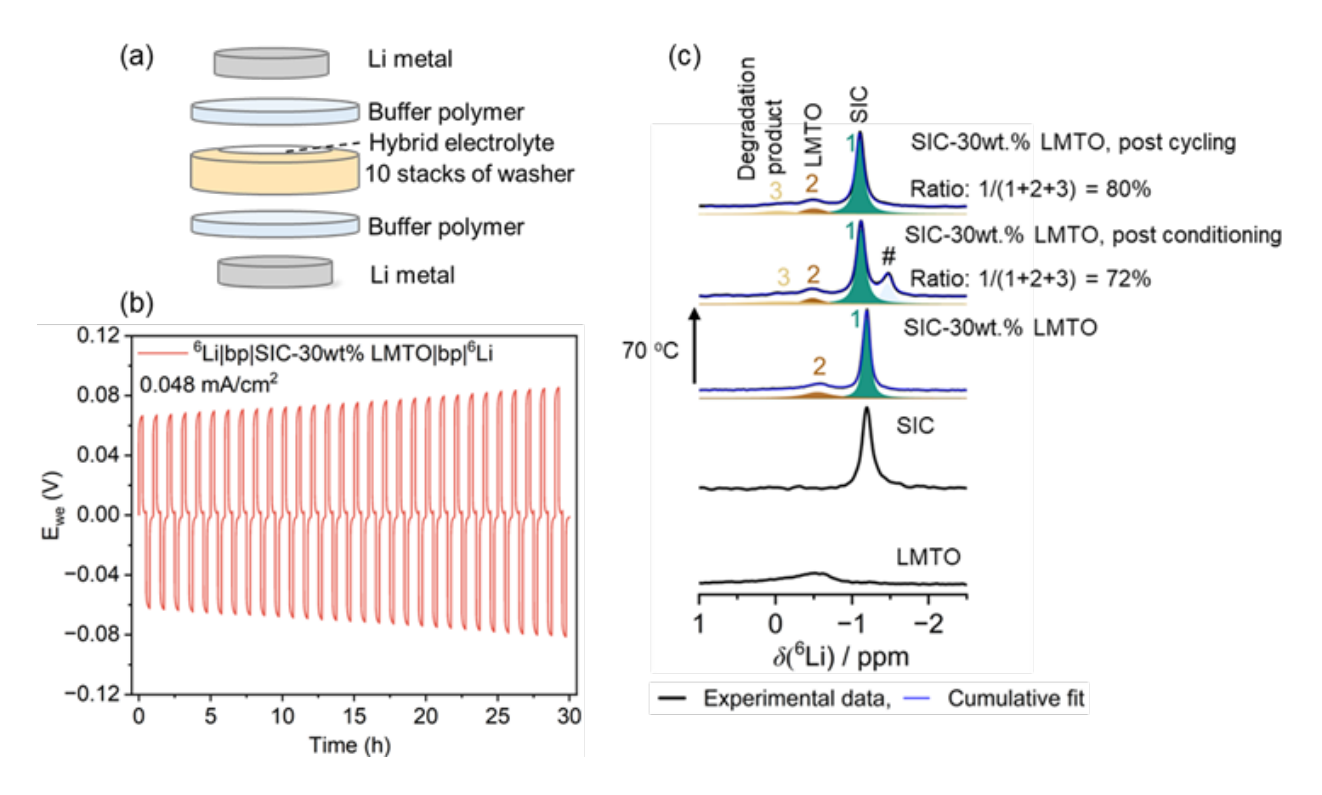


Figure 2. (a) Schematic and (b) electrochemical profiles of the [⁶Li|buffer polymer|SIC-30wt.% LMTO composite|buffer polymer|⁶Li] symmetric cell when cycled at a constant current of 0.048 mA/cm² at 70 °C for 30 cycles. (c) ⁶Li solid-state NMR spectra collected at 18.8 T, 30 °C and 30 kHz magic angle spinning (MAS) on the pure LMTO and SIC components, on the pure hybrid electrolyte, and on the hybrid electrolyte (+ buffer polymer layer) extracted from the cell after conditioning and after cycling.

As mentioned earlier, the results from our tracer exchange experiments are only valid and quantitative if Li chemical exchange between the bulk of the SIC polymer, the interface, and the LMTO ceramic is negligible on the timescale of the analysis of *ex situ* cycled samples (i.e., no Li chemical exchange occurs between different regions of the sample in days). We thus set out to probe chemical exchange over a range of timescales from milliseconds to days. To probe Li chemical exchange on the order of milliseconds to seconds, 2D ⁶Li EXSY NMR experiments were conducted at 80 °C and 60 °C on a higher LMTO loading (SIC-50wt.% LMTO) composite electrolyte to facilitate the observation of the ⁶Li signal from the LMTO component, with results shown in **Figures 3** and **S4**, respectively.

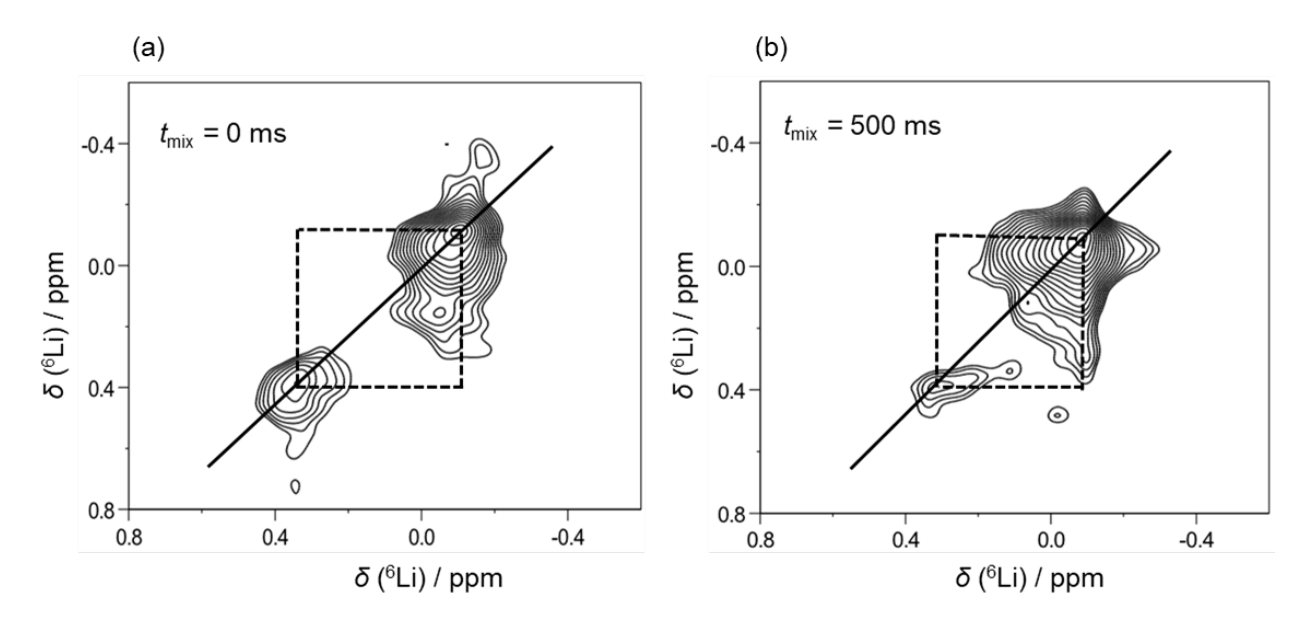


Figure 3. Two-dimensional 6 Li- 6 Li EXSY spectra collected on the SIC-50wt.% LMTO hybrid electrolyte acquired with (a) 0 ms and (b) 500 ms mixing times (t_{mix}) at 18.8 T, 80°C and 30 kHz MAS.

If chemical exchange takes place between the SIC and LMTO components of the hybrid electrolyte on the order of the mixing time (t_{mix}) used in the EXSY experiment, the 2D spectrum will show off-diagonal (cross) peaks relating the SIC and LMTO resonances on the diagonal. Here, we see no evidence of cross peaks in the spectra collected at 80 °C up to a t_{mix} of 500 milliseconds (**Figure 3**), and in the spectra collected at 60 °C up to a t_{mix} of 3 seconds (**Figure S4**). These measurements are, however, limited in sensitivity due to the weak LMTO signal intensity, and can only probe chemical exchange over timescales shorter than the longitudinal (T_1) relaxation time of the SIC and LMTO signals (of 12 s and 8 s respectively at 80 °C). In other words, these measurements do not rule out Li chemical exchange between the SIC and LMTO components on the order of tens of seconds, hours, or even days, that would still compromise the outcome of the tracer exchange experiments.

We next probe longer exchange timescales using a new isotope exchange experiment. In this experiment, 50 wt.% ⁶Li-enriched LMTO was mixed with VEC and natural-abundance MTFSILi. The mixture was heated for 12 hours at 80 °C in a nitrogen-filled glovebox to initiate polymerization and form the SIC-50 wt% ⁶Li-enriched LMTO composite. Any Li chemical exchange taking place between the SIC, serving as a source of ⁷Li, and the LMTO particles should lead to progressive ⁷Li enrichment of those particles and the appearance and growth over time of

a new resonance associated with the LMTO phase in the ⁷Li solid-state NMR spectrum. After the initial 12-hour polymerization step at 80 °C, the SIC-50 wt.% ⁶Li-enriched LMTO composite was transferred to a 2.5 mm NMR rotor. To confirm that 6Li-enriched LMTO does not affect the polymerization process, a ⁷Li solid-state NMR spectrum was collected at 30 °C and is compared in Figure S5 to the spectrum obtained at the same temperature on the SIC-30wt.% LMTO (at natural abundance) sample used for the tracer exchange measurement. As expected, no signal is observed from the 6Li-enriched LMTO component, and the two SIC polymer resonances show very similar shifts, indicating that the ⁶Li-enriched ceramic precursor does not impact the polymerization process. Proceeding with the isotope exchange experiment, the SIC-50 wt.% ⁶Lienriched LMTO composite sample was then equilibrated inside the NMR probe at 80 °C for 20 minutes before acquiring the first spectrum of the series at "t = 0 min". The ⁷Li solid-state NMR spectra collected at regular intervals over the course of 2 days are presented in Figure 4 (the chemical shifts and integrated intensities of the resonances are listed in Table S3). The SIC resonance observed at -0.51 ppm at t = 0 min shifts to -0.39 ppm over the first 40 minutes, and then more slowly to -0.33 ppm over the course of 48 h (Table S3). Additionally, the integrated intensity gradually decreases as it broadens over time. The evolution of the lineshape of the SIC resonance is consistent with the gradual decrease of its transverse (T_2) relaxation time ($T_2 = 20$ ms at t = 0 min and $T_2 = 12$ ms at t = 48 h). All in all, the decreasing T_2 time and gradual shift of the SIC signal suggest further in situ polymerization of the composite electrolyte over the course of the NMR measurement. The gradual shift of the SIC signal should not affect the interpretation of the isotope exchange experiment as the separation between the SIC and LMTO signals is sufficiently large (of 0.6 ppm from the 30 °C 7Li solid-state NMR data shown in Figure S5, which is larger than the linewidth of the ⁷Li SIC signal observed here) that any LMTO signal that may appear over the course of the measurement should be well separated from the SIC signal. Since no new ⁷Li resonance was detected up to 48 h after the sample was equilibrated at 80 °C inside the NMR probe, we conclude that there is no significant Li chemical exchange between the SIC and LMTO components on this timescale. Finally, we note a downfield shift of the ⁷Li SIC resonance recorded at 80°C compared to the ⁷Li SIC resonance recorded at 30 °C in Figure S5, which we attribute to the change in temperature of the shim coil, affecting spectral calibration. Since the change in shim coil temperature leads to a solid shift of all NMR signals, this does not affect the results from the isotope exchange measurement.

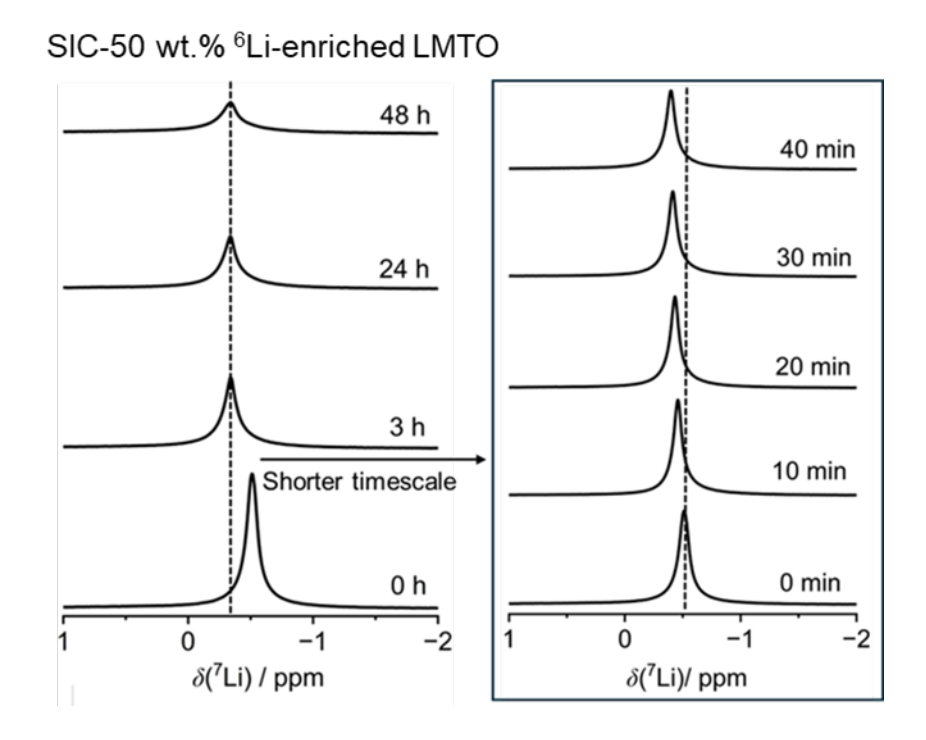


Figure 4. Evolution of the ⁷Li NMR spectrum obtained on the SIC-50wt.% ⁶Li-enriched LMTO composite electrolyte with time. The inset shows the evolution of the ⁷Li NMR spectrum over the first 40 minutes. All experiments were conducted on the same composite sample maintained at 80 °C throughout, at 18.8 T and 30 kHz MAS.

The EXSY and isotope exchange results confirm that Li chemical exchange between the SIC polymer and the LMTO ceramic is in the "ultraslow" regime (Figure 1b), *i.e.*, that the tracer exchange results on the SIC-50wt.% LMTO electrolyte (Figure 2c) are quantitative. Together, these results suggest that the increased ionic conductivity of the hybrid electrolyte relative to the pure polymer is due to improved (low energy barrier) Li-ion transport in the interfacial region of the polymer. The LMTO nanorods presumably weaken the electrostatic interactions between Li-ion and the polyanion, as has been observed for silica and alumina fillers [55,56], and do not contribute directly to the Li-ion conductivity. That is, they act as a passive filler. The question then arises as to the limit of the conductivity enhancements that can be achieved when using a passive filler. Can the conductivity be enhanced 10- or 100-fold? While there is no definite answer to this day, previous work on model nanocomposites [57–59] have indicated that polymer properties (*e.g.*, density, chain packing, structural relaxation and mechanical properties) can be modulated over length scales on the order of a few nanometers around ceramic particles. Further, these changes in properties are rather subtle, and while they are consistent with the two- to three-fold increase in

Li-ion transport observed in the SIC-LMTO composite electrolytes of interest to this work, achieving 10- or 100-fold conductivity enhancements using this strategy is highly unlikely. Overall, fundamental studies are needed to better understand the limits of composite polymer electrolyte design involving passive fillers.

The use of a ceramic filler exhibiting a significantly higher ionic conductivity than the polymer matrix remains the most efficient method to boost the conductivity of the composite electrolyte. As we have seen in this work, an additional criterion for long-range conduction through both the bulk ceramic and polymer regions is fast ion exchange at the polymer-ceramic interfaces. While recent studies have demonstrated that Li can exchange between an organic liquid electrolyte or polymer matrix (e.g., PEO) and a superionic ceramic (e.g., argyrodite Li₆PS₅Cl, Li_(1+x)Al_xTi₍₂₋ $_{x}$ (PO₄)₃ (LATP)) [60–62], there has been no discussion as to whether this exchange occurs on a sufficiently short timescale for the ceramic itself to play a role in long-range ion transport in the hybrid electrolyte. Hence, we introduce the idea of a critical interfacial ion exchange time for the bulk ceramic to be involved in the conduction process. To derive an expression for this critical time, t_c , we consider a hybrid electrolyte comprising a superionic ceramic with an ionic conductivity that significantly exceeds that of the polymer matrix but with no continuous path between the ceramic particles, and compare the Li diffusion time through the polymer matrix alone (t_p) and through a discontinuous (polymer-ceramic-polymer) region (t_d) over a distance on the order of the average ceramic particle size (L). An illustrative diagram is provided in **Figure S6.** The diffusion time t_p can once again be derived from the Einstein-Smoluchowski relation in three dimensions, and $t_p = \frac{L^2}{6D} \sim \frac{L^2}{D}$. The diffusion time for a path through a filler particle, t_d , is the sum over the diffusion time within the ceramic particle of length $L\left(t_{cer}\right)$ and twice the interfacial exchange time (t_{exc}) , assuming a symmetrical interfacial exchange rate: $t_d = t_{cer} + 2t_{exc}$. This expression can further be simplified to $t_d \sim t_{exc}$, assuming that Li-ion transport across the interface is rate-limiting and dropping the factor of 2. The critical interfacial ion exchange time t_c corresponds to the value of t_{exc} when diffusion through the discontinuous region equals that through the polymer matrix: $t_d \sim t_p$, hence $t_c \sim \frac{L^2}{D}$.

We now evaluate the critical ion interfacial exchange time for the SIC-LMTO composite electrolyte of interest to this work, and for several other hybrid electrolytes from the few reports

that, to the best of our knowledge, provided all necessary parameters for the calculation. As mentioned earlier, for the SIC-50wt.% LMTO composite, an average room temperature ⁷Li selfdiffusion coefficient on the order of $D \sim 10^{-12} \, m^2/s$ was obtained for transport within the polymer matrix [41]. Considering LMTO nanorods with $L \sim 150 \, nm$, we derive a critical exchange time of 22.5 ms. In this case, Li interfacial exchange should occur on the order of a millisecond for the ceramic to contribute to the overall conductivity of the hybrid electrolyte. Recently, McCloskey and coworkers investigated a hybrid organic liquid-LATP electrolyte and showed that interfacial ion exchange takes place on the order of a few minutes when using LATP particles with a particle size $L \sim 1 \,\mu m$, and on the order of 30 minutes for $L \sim 10 \,\mu m$ [60]. They further derived room temperature Li self-diffusion coefficients on the order of $D \sim 10^{-12} m^2/s$ for these hybrid electrolytes, resulting in a critical exchange time $t_c \sim \frac{L^2}{D} \sim 1$ s for the electrolyte comprising 1 μm -particles and ~100 s for the electrolyte comprising 10 μm - particles. These times are significantly shorter than the ion exchange times, which explains why only a slight increase in conductivity was observed upon addition of the LATP nanoparticles to the electrolytic solution [60]. Similarly, Martinez-Ibanez and coworkers examined Li-ion transport in a composite electrolyte comprising LiTFSI-doped poly(ethylene oxide – propylene oxide) (P(EO-PO)) and LATP particles, where the copolymer matrix was plasticized with PEGDME to further improve conductivity [62]. Using EXSY, the characteristic polymer-ceramic Li exchange time was estimated to be short, on the order of 50 ms at 60 °C and 300 ms at 20 °C. The authors reported an average LATP particle size of $\sim 0.7 \ \mu m$, and an average Li self-diffusion coefficient of $\sim 4 \times$ $10^{-12}m^2/s$ at 60 °C and ~ $10^{-12}m^2/s$ at 20 °C. From these results, we derive critical exchange times of $\sim 120 \text{ ms}$ at 60 °C and $\sim 500 \text{ ms}$ at T = 20 °C, which are slightly longer than the observed interfacial exchange times at each temperature, suggesting that the ceramic particles contribute to the overall conductivity. However, no increase in bulk conductivity was observed upon adding the ceramic although the Li transference number increased slightly [62]. This could be because the ionic conductivity of LATP is comparable to that of the copolymer matrix.

Overall, our results and this discussion highlight the critical role of polymer-ceramic interfacial ion exchange in the design of hybrid electrolytes, and the need to better understand the parameters controlling interfacial migration energy barriers. We argue that, to achieve significant conductivity enhancements in composite electrolytes, the superionic ceramic particles must also enable fast ion

exchange at polymer-ceramic interfaces. Specifically, to leverage the ion transport properties of active ceramic particles, the interfacial exchange time plus the Li diffusion time through a ceramic particle must be shorter than or equal to the Li diffusion time through the polymer phase over distances on the order of the average particle size. If the rate of interfacial ion exchange is too low, ions will choose the path of least resistance and diffuse through the polymer phase, and the ceramic particles will not actively participate in ion transport. Those particles may still increase the ionic conductivity and cation transport number of the composite electrolyte, but we suggest that these improvements will not be significant.

4. Conclusions

This study provided critical insights into lithium (Li)-ion transport pathways in a bis[(trifluoromethyl)sulfonyl]imide (MTFSI)-vinyl ethylene carbonate (VEC)-based single-ion conducting (SIC) polymer electrolyte using various solid-state NMR techniques. ⁶Li→⁷Li tracer exchange NMR spectroscopy indicated that Li preferentially migrates through the SIC polymer or the polymer interfacial region. ⁶Li exchange spectroscopy (EXSY) and a new isotope exchange NMR method revealed the absence of Li exchange between the polymer and ceramic regions of the composite on the second timescale and on the timescale of days, respectively, at 80 °C. These results confirmed that Li-conductive LMTO nanorods act as a passive filler and likely enhance conductivity by reducing electrostatic interactions between Li-ions and the polyanion matrix. As an extension of this work, we considered the key requirements for significant improvements in the transport properties of a polymer matrix through addition of ceramic fillers. We argued that filler particles with an ionic conductivity that is significantly higher than that of the polymer matrix are essential to the development of high conductivity polymer-ceramic composite electrolytes, but an additional requirement is fast interfacial ion exchange. This led us to introduce a new criterion, the critical interfacial ion exchange time, to determine whether ceramic particles actively participate in long-range ion transport in a composite electrolyte. These findings provide a framework for screening polymer-ceramic pairings that may enable significant conductivity improvements and accelerate the development of next-generation, solid-state batteries.

Supporting Information

Electrochemical profile of the symmetric cell, 1D ⁶Li solid-state NMR, 2D ⁶Li-⁶Li EXSY collected at 60 °C, ⁷Li tracer exchange NMR data and Tables containing ^{6/7}Li isotopic chemical shifts and integrated intensities.

AUTHOR INFORMATION

Corresponding Authors

Raphaële J. Clément – Materials Department and Materials Research Laboratory, University of California, Santa Barbara, California, 93106, United States; ORCID: https://orcid.org/0000-0002-3611-1162; Email: rclement@ucsb.edu

Xi Chelsea Chen – Chemical Sciences Division, Oak Ridge National Laboratory, 1 Bethel Valley Road, Oak Ridge, TN, 37830, United States; ORCID: https://orcid.org/0000-0003-1188-7658; Email: chenx@ornl.gov

Alexei Sokolov – sokolov@utk.edu, Chemical Sciences Division, Oak Ridge National Laboratory, 1 Bethel Valley Road, Oak Ridge, TN, 37830, United States; ORCID: https://orcid.org/0000-0002-8187-9445; Email: sokolov@utk.edu

Authors

Amit Bhattacharya – Materials Department and Materials Research Laboratory, University of California Santa Barbara, Santa Barbara, California, 93106, United States; ORCID: https://orcid.org/0000-0002-3104-9187

Ji-young Ock – Chemical Sciences Division, Oak Ridge National Laboratory, 1 Bethel Valley Road, 37830, United States; ORCID: https://orcid.org/0000-0002-1159-1753

Tao Wang – Chemical Sciences Division, Oak Ridge National Laboratory, 1 Bethel Valley Road, 37830, United States; ORCID: https://orcid.org/0000-0001-5004-160X

Road, 37830, United States; ORCID: https://orcid.org/0000-0001-8379-259X

Sheng Dai – Chemical Sciences Division, Oak Ridge National Laboratory, 1 Bethel Valley Road, 37830, United States; ORCID: https://orcid.org/0000-0002-8046-3931

James T. Bamford-Materials Department and Department of Chemical Engineering, University of California, Santa Barbara, California 93106, United States; https://orcid.org/0000-0002-0444-0666

Rachel A. Segalman– Materials Department and Department of Chemical Engineering, University of California, Santa Barbara, California 93106, United States; https://orcid.org/0000-0002-4292-5103

Notes

The authors declare no competing financial interest.

Acknowledgements

This work was supported as part of the Fast and Cooperative Ion Transport in Polymer-Based Materials (FaCT), an Energy Frontier Research Center funded by the U.S. Department of Energy, Office of Science, Basic Energy Sciences at Oak Ridge National Laboratory. The research reported here made use of the shared facilities of the Materials Research Science and Engineering Center (MRSEC) at UC Santa Barbara: NSF DMR-2308708. The UC Santa Barbara MRSEC is a member of the Materials Research Facilities Network (www.mrfn.com). A.B. and R.J.C thank Prof. Michal Leskes and Dr. Leo W. Gordon for helpful scientific discussions, and Dr. Valentino R. Cooper for his contributions to the revision of the manuscript.

References

- [1] J.B. Goodenough, K.-S. Park, The Li-ion rechargeable battery: a perspective, J. Am. Chem. Soc. 135 (2013) 1167–1176. https://doi.org/10.1021/ja3091438.
- [2] Y. Kato, S. Hori, T. Saito, K. Suzuki, M. Hirayama, A. Mitsui, M. Yonemura, H. Iba, R. Kanno, High-power all-solid-state batteries using sulfide superionic conductors, Nat. Energy 1 (2016) 1–7. https://doi.org/10.1038/nenergy.2016.30.
- [3] Y. Liu, Y. Zhu, Y. Cui, Challenges and opportunities towards fast-charging battery materials, Nat. Energy 4 (2019) 540–550. https://doi.org/10.1038/s41560-019-0405-3.
- [4] A. Manthiram, An outlook on lithium ion battery technology, ACS Cent. Sci. 3 (2017) 1063–1069. https://doi.org/10.1021/acscentsci.7b00288.
- [5] S. Lou, F. Zhang, C. Fu, M. Chen, Y. Ma, G. Yin, J. Wang, Interface issues and challenges in all-solid-state batteries: lithium, sodium, and beyond, Adv. Mater. 33 (2021) 2000721. https://doi.org/10.1002/adma.202000721.
- [6] L. Xu, S. Tang, Y. Cheng, K. Wang, J. Liang, C. Liu, Y.-C. Cao, F. Wei, L. Mai, Interfaces in solid-state lithium batteries, Joule 2 (2018) 1991–2015. https://doi.org/10.1016/j.joule.2018.07.009.
- [7] L. Wang, A. Menakath, F. Han, Y. Wang, P.Y. Zavalij, K.J. Gaskell, O. Borodin, D. Iuga, S.P. Brown, C. Wang, K. Xu, B.W. Eichhorn, Identifying the components of the solid–electrolyte interphase in Li-ion batteries, Nat. Chem. 11 (2019) 789–796. https://doi.org/10.1038/s41557-019-0304-z.
- [8] M. Ma, M. Zhang, B. Jiang, Y. Du, B. Hu, C. Sun, A review of all-solid-state electrolytes for lithium batteries: high-voltage cathode materials, solid-state electrolytes and electrode-electrolyte interfaces, Mater. Chem. Front. 7 (2023) 1268–1297. https://doi.org/10.1039/D2QM01071B.
- [9] M. Armand, Polymer solid electrolytes an overview, Solid State Ion. 9–10 (1983) 745–754. https://doi.org/10.1016/0167-2738(83)90083-8.
- [10] Y. Kato, M. Watanabe, K. Sanui, N. Ogata, Ionic transport number of network PEO electrolytes, Solid State Ion. 40–41 (1990) 632–636. https://doi.org/10.1016/0167-2738(90)90085-6.
- [11] L. Long, S. Wang, M. Xiao, Y. Meng, Polymer electrolytes for lithium polymer batteries, J. Mater. Chem. A 4 (2016) 10038–10069. https://doi.org/10.1039/C6TA02621D.

- [12] K.P. Barteau, M. Wolffs, N.A. Lynd, G.H. Fredrickson, E.J. Kramer, C.J. Hawker, Allyl glycidyl ether-based polymer electrolytes for room temperature lithium batteries, Macromolecules 46 (2013) 8988–8994. https://doi.org/10.1021/ma401267w.
- [13] D. Zhou, D. Shanmukaraj, A. Tkacheva, M. Armand, G. Wang, Polymer electrolytes for lithium-based batteries: advances and prospects, Chem 5 (2019) 2326–2352. https://doi.org/10.1016/j.chempr.2019.05.009.
- [14] Y. Zheng, Y. Yao, J. Ou, M. Li, D. Luo, H. Dou, Z. Li, K. Amine, A. Yu, Z. Chen, A review of composite solid-state electrolytes for lithium batteries: fundamentals, key materials and advanced structures, Chem. Soc. Rev. 49 (2020) 8790–8839. https://doi.org/10.1039/D0CS00305K.
- [15] E. van der Maas, W. Zhao, Z. Cheng, T. Famprikis, M. Thijs, S.R. Parnell, S. Ganapathy, M. Wagemaker, Investigation of structure, ionic conductivity, and electrochemical stability of halogen substitution in solid-state ion conductor Li₃YBr_xCl_{6-x}, J. Phys. Chem. C 127 (2023) 125–132. https://doi.org/10.1021/acs.jpcc.2c07910.
- [16] Y. Inaguma, C. Liquan, M. Itoh, T. Nakamura, T. Uchida, H. Ikuta, M. Wakihara, High ionic conductivity in lithium lanthanum titanate, Solid State Commun. 86 (1993) 689–693. https://doi.org/10.1016/0038-1098(93)90841-A.
- [17] J. Janek, W.G. Zeier, A solid future for battery development, Nat. Energy 1 (2016) 16141. https://doi.org/10.1038/nenergy.2016.141.
- [18] T. Ye, L. Li, Y. Zhang, Recent progress in solid electrolytes for energy storage devices, Adv. Funct. Mater. 30 (2020) 2000077. https://doi.org/10.1002/adfm.202000077.
- [19] D. Spencer Jolly, D.L.R. Melvin, I.D.R. Stephens, R.H. Brugge, S.D. Pu, J. Bu, Z. Ning, G.O. Hartley, P. Adamson, P.S. Grant, A. Aguadero, P.G. Bruce, Interfaces between ceramic and polymer electrolytes: a comparison of oxide and sulfide solid electrolytes for hybrid solid-state batteries, Inorganics 10 (2022) 60. https://doi.org/10.3390/inorganics10050060.
- [20] P. Barai, T. Fuchs, E. Trevisanello, F.H. Richter, J. Janek, V. Srinivasan, Study of void formation at the lithium|solid electrolyte interface, Chem. Mater. 36 (2024) 2245–2258. https://doi.org/10.1021/acs.chemmater.3c01708.
- [21] Y. Lu, C.-Z. Zhao, J.-K. Hu, S. Sun, H. Yuan, Z.-H. Fu, X. Chen, J.-Q. Huang, M. Ouyang, Q. Zhang, The void formation behaviors in working solid-state Li metal batteries, Sci. Adv. 8 (2022) eadd0510. https://doi.org/10.1126/sciadv.add0510.

- [22] M.H. Bocanegra-Bernal, Hot isostatic pressing (HIP) technology and its applications to metals and ceramics, J. Mater. Sci. 39 (2004) 6399–6420.https://doi.org/10.1023/B:JMSC.0000044878.11441.90.
- [23] T.A. Yersak, F. Hao, C. Kang, J.R. Salvador, Q. Zhang, H.J.G. Malabet, M. Cai, Consolidation of composite cathodes with NCM and sulfide solid-state electrolytes by hot pressing for all-solid-state Li metal batteries, J. Solid State Electrochem. 26 (2022) 709–718. https://doi.org/10.1007/s10008-021-05104-8.
- [24] D.G. Mackanic, X. Yan, Q. Zhang, N. Matsuhisa, Z. Yu, Y. Jiang, T. Manika, J. Lopez, H. Yan, K. Liu, X. Chen, Y. Cui, Z. Bao, Decoupling of mechanical properties and ionic conductivity in supramolecular lithium ion conductors, Nat. Commun. 10 (2019) 5384. https://doi.org/10.1038/s41467-019-13362-4.
- [25] M. Singh, O. Odusanya, G.M. Wilmes, H.B. Eitouni, E.D. Gomez, A.J. Patel, V.L. Chen, M.J. Park, P. Fragouli, H. Iatrou, N. Hadjichristidis, D. Cookson, N.P. Balsara, Effect of molecular weight on the mechanical and electrical properties of block copolymer electrolytes, Macromolecules 40 (2007) 4578–4585. https://doi.org/10.1021/ma0629541
- [26] H. Kosonen, S. Valkama, J. Hartikainen, H. Eerikäinen, M. Torkkeli, K. Jokela, R. Serimaa, F. Sundholm, G. Ten Brinke, O. Ikkala, Mesomorphic structure of poly(styrene)- *block* poly(4-vinylpyridine) with oligo(ethylene oxide)sulfonic acid side chains as a model for molecularly reinforced polymer electrolyte, Macromolecules 35 (2002) 10149–10154. https://doi.org/10.1021/ma0201577.
- [27] M.W. Schulze, L.D. McIntosh, M.A. Hillmyer, T.P. Lodge, High-Modulus, High-conductivity nanostructured polymer electrolyte membranes via polymerization-induced phase separation, Nano Lett. 14 (2014) 122–126. https://doi.org/10.1021/nl4034818.
- [28] S. Choudhury, R. Mangal, A. Agrawal, L.A. Archer, A highly reversible room-temperature lithium metal battery based on crosslinked hairy nanoparticles. Nat Commun 6: 10101, 2015.
- [29] J.T. Bamford, S.D. Jones, N.S. Schauser, B.J. Pedretti, L.W. Gordon, N.A. Lynd, R.J. Clément, R.A. Segalman, Improved mechanical strength without sacrificing Li-ion transport in polymer electrolytes, ACS Macro Lett. 13 (2024) 638-643. https://doi.org/10.1021/acsmacrolett.4c00158.

- [30] C. Wang, W. Li, D. Li, X. Zhao, Y. Li, Y. Zhang, X. Qi, M. Wu, L.-Z. Fan, High-performance solid-state lithium metal batteries of garnet/polymer composite thin-film electrolyte with domain-limited ion transport pathways, ACS Nano 18 (2024) 32175–32185. https://doi.org/10.1021/acsnano.4c11205.
- [31] X. Yang, J. Liu, N. Pei, Z. Chen, R. Li, L. Fu, P. Zhang, J. Zhao, The critical role of fillers in composite polymer electrolytes for lithium battery, Nano-Micro Lett. 15 (2023) 74. https://doi.org/10.1007/s40820-023-01051-3.
- [32] W. Liu, S.W. Lee, D. Lin, F. Shi, S. Wang, A.D. Sendek, Y. Cui, Enhancing ionic conductivity in composite polymer electrolytes with well-aligned ceramic nanowires, Nat. Energy 2 (2017) 1–7. https://doi.org/10.1038/nenergy.2017.35.
- [33] F. Croce, G.B. Appetecchi, L. Persi, B. Scrosati, Nanocomposite polymer electrolytes for lithium batteries, Nature 394 (1998) 456–458. https://doi.org/10.1038/28818.
- [34] W. Liu, N. Liu, J. Sun, P.-C. Hsu, Y. Li, H.-W. Lee, Y. Cui, Ionic conductivity enhancement of polymer electrolytes with ceramic nanowire fillers, Nano Lett. 15 (2015) 2740–2745. https://doi.org/10.1021/acs.nanolett.5b00600.
- [35] L.-Z. Fan, H. He, C.-W. Nan, Tailoring inorganic-polymer composites for the mass production of solid-state batteries, Nat. Rev. Mater. 6 (2021) 1003-1019. https://doi.org/10.1038/s41578-021-00320-0.
- [36] V.P. Hoang Huy, S. So, J. Hur, Inorganic fillers in composite gel polymer electrolytes for high-performance lithium and non-lithium polymer batteries, Nanomaterials 11 (2021) 614. https://doi.org/10.3390/nano11030614.
- [37] Y. Horowitz, M. Lifshitz, A. Greenbaum, Y. Feldman, S. Greenbaum, A.P. Sokolov, D. Golodnitsky, Review—polymer/ceramic interface barriers: the fundamental challenge for advancing composite solid electrolytes for Li-ion batteries, J. Electrochem. Soc. 167 (2020) 160514. https://doi.org/10.1149/1945-7111/abcd12.
- [38] X.C. Chen, X. Liu, A. Samuthira Pandian, K. Lou, F.M. Delnick, N.J. Dudney, Determining and minimizing resistance for ion transport at the polymer/ceramic electrolyte interface, ACS Energy Lett. 4 (2019) 1080–1085. https://doi.org/10.1021/acsenergylett.9b00495.

- [39] X.C. Chen, R.L. Sacci, N.C. Osti, M. Tyagi, Y. Wang, M.J. Palmer, N.J. Dudney, Study of segmental dynamics and ion transport in polymer-ceramic composite electrolytes by quasi-elastic neutron scattering, Mol. Syst. Des. Eng. 4 (2019) 379–385. https://doi.org/10.1039/C8ME00113H.
- [40] J. Peng, Y. Xiao, D.A. Clarkson, S.G. Greenbaum, T.A. Zawodzinski, X.C. Chen, A nuclear magnetic resonance study of cation and anion dynamics in polymer–ceramic composite solid electrolytes, ACS Appl. Polym. Mater. 2 (2020) 1180–1189. https://doi.org/10.1021/acsapm.9b01068.
- [41] J. Ock, A. Bhattacharya, T. Wang, C. Gainaru, Y. Wang, K.L. Browning, M. Lehmann, M.A. Rahman, M. Chi, F. Wang, J.K. Keum, L. Kearney, T. Saito, S. Dai, R.J. Clément, A.P. Sokolov, X.C. Chen, Percolating interfacial layers enhance conductivity in polymer-composite electrolytes, Macromolecules 57 (2024) 7489-7498.https://doi.org/10.1021/acs.macromol.4c00615.
- [42] T. Wang, J. Ock, X.C. Chen, F. Wang, M. Li, M.S. Chambers, G.M. Veith, L.B. Shepard, S.B. Sinnott, A. Borisevich, M. Chi, A. Bhattacharya, R.J. Clément, A.P. Sokolov, S. Dai, Flux synthesis of A-site disordered perovskite La_{0.5}M_{0.5}TiO₃ (M = Li, Na, K) nanorods tailored for solid composite electrolytes, Adv. Sci. 12 (2025) 2408805. https://doi.org/10.1002/advs.202408805.
- [43] S. Kobayashi, D. Yokoe, Y. Fujiwara, K. Kawahara, Y. Ikuhara, A. Kuwabara, Lithium lanthanum titanate single crystals: dependence of lithium-ion conductivity on crystal domain orientation, Nano Lett. 22 (2022) 5516–5522. https://doi.org/10.1021/acs.nanolett.2c01655.
- [44] S. Stramare, V. Thangadurai, W. Weppner, Lithium lanthanum titanates: a review, Chem. Mater. 15 (2003) 3974–3990. https://doi.org/10.1021/cm0300516.
- [45] J. Zheng, P. Wang, H. Liu, Y.-Y. Hu, Interface-enabled ion conduction in Li₁₀GeP₂S₁₂ Poly(ethylene Oxide) hybrid electrolytes, ACS Appl. Energy Mater. 2 (2019) 1452–1459. https://doi.org/10.1021/acsaem.8b02008.
- [46] J. Zheng, H. Dang, X. Feng, P.-H. Chien, Y.-Y. Hu, Li-ion transport in a representative ceramic–polymer–plasticizer composite electrolyte: Li₇La₃Zr₂O₁₂–polyethylene oxide–tetraethylene glycol dimethyl ether, J. Mater. Chem. A 5 (2017) 18457–18463. https://doi.org/10.1039/C7TA05832B.

- [47] J. Zheng, M. Tang, Y.-Y. Hu, Lithium ion pathway within Li₇La₃Zr₂O₁₂-polyethylene oxide composite electrolytes, Angew. Chem. Int. Ed. 55 (2016) 12538–12542. https://doi.org/10.1002/anie.201607539.
- [48] X. Feng, P.-H. Chien, S. Patel, J. Zheng, M. Immediato-Scuotto, Y. Xin, I. Hung, Z. Gan, Y.-Y. Hu, Synthesis and characterizations of highly conductive and stable electrolyte Li₁₀P₃S₁₂I, Energy Storage Mater. 22 (2019) 397–401. https://doi.org/10.1016/j.ensm.2019.07.047.
- [49] T. Yang, J. Zheng, Q. Cheng, Y.-Y. Hu, C.K. Chan, Composite polymer electrolytes with Li₇La₃Zr₂O₁₂ garnet-type nanowires as ceramic fillers: mechanism of conductivity enhancement and role of doping and morphology, ACS Appl. Mater. Interfaces 9 (2017) 21773–21780. https://doi.org/10.1021/acsami.7b03806.
- [50] R.K. Harris, E.D. Becker, S.M.C. de Menezes, R. Goodfellow, P. Granger, NMR nomenclature. Nuclear spin properties and conventions for chemical shifts (IUPAC Recommendations 2001), Pure Appl. Chem. 73 (2001) 1795–1818. https://doi.org/10.1351/pac200173111795.
- [51] M.H. Levitt, Spin Dynamics: Basics of Nuclear Magnetic Resonance, John Wiley & Sons, 2008.
- [52] R. Sahore, K.D. Owensby, B.L. Armstrong, J. Ock, M.L. Lehmann, A.M. Ullman, S. Kalnaus, X.C. Chen, Pathway to high rate capability in interconnected composite electrolytes: a case study with a single-ion-conducting polymer, ACS Appl. Energy Mater. 7 (2024) 11714–11723. https://doi.org/10.1021/acsaem.4c01642.
- [53] H. Liu, P. He, G. Wang, Y. Liang, C. Wang, L.-Z. Fan, Thin, flexible sulfide-based electrolyte film and its interface engineering for high performance solid-state lithium metal batteries, Chem. Eng. J. 430 (2022) 132991. https://doi.org/10.1016/j.cej.2021.132991.
- [54] K.D. Owensby, J. Ock, R. Sahore, H.M.I. Meyer, E.C. Self, Y.-R. Lin, W.-Y. Tsai, X.C. Chen, The Impact of lithium anode interface on capacity fade in polymer electrolyte-based solid-state batteries, ACS Appl. Energy Mater. 7 (2024) 10271–10280. https://doi.org/10.1021/acsaem.4c01350.
- [55] C. Wang, T. Yang, W. Zhang, H. Huang, Y. Gan, Y. Xia, X. He, J. Zhang, Hydrogen bonding enhanced SiO₂ /PEO composite electrolytes for solid-state lithium batteries, J. Mater. Chem. A 10 (2022) 3400–3408. https://doi.org/10.1039/D1TA10607D.

- [56] J. Li, M. Jing, R. Li, L. Li, Z. Huang, H. Yang, M. Liu, S. Hussain, J. Xiang, X. Shen, Al₂O₃ Fiber-reinforced polymer solid electrolyte films with excellent lithium-ion transport properties for high-voltage solid-state lithium batteries, ACS Appl. Polym. Mater. 4 (2022) 7144–7151. https://doi.org/10.1021/acsapm.2c01034.
- [57] A.P. Holt, P.J. Griffin, V. Bocharova, A.L. Agapov, A.E. Imel, M.D. Dadmun, J.R. Sangoro, A.P. Sokolov, Dynamics at the polymer/nanoparticle interface in poly(2-vinylpyridine)/silica nanocomposites, Macromolecules 47 (2014) 1837–1843. https://doi.org/10.1021/ma5000317.
- [58] S. Cheng, B. Carroll, V. Bocharova, J.-M. Carrillo, B.G. Sumpter, A.P. Sokolov, Focus: Structure and dynamics of the interfacial layer in polymer nanocomposites with attractive interactions, J. Chem. Phys. 146 (2017) 203201. https://doi.org/10.1063/1.4978504.
- [59] A.-C. Genix, V. Bocharova, A. Kisliuk, B. Carroll, S. Zhao, J. Oberdisse, A.P. Sokolov, Enhancing the mechanical properties of glassy nanocomposites by tuning polymer molecular weight, ACS Appl. Mater. Interfaces 10 (2018) 33601–33610. https://doi.org/10.1021/acsami.8b13109.
- [60] D. Yu, Z.C. Tronstad, B.D. McCloskey, Lithium-ion transport and exchange between phases in a concentrated liquid electrolyte containing lithium-ion-conducting inorganic particles, ACS Energy Lett. 9 (2024) 1717-1724. https://doi.org/10.1021/acsenergylett.4c00502.
- [61] M. Liu, S. Zhang, E.R.H. van Eck, C. Wang, S. Ganapathy, M. Wagemaker, Improving Liion interfacial transport in hybrid solid electrolytes, Nat. Nanotechnol. 17 (2022) 959–967. https://doi.org/10.1038/s41565-022-01162-9.
- [62] N. Boaretto, P. Ghorbanzade, H. Perez-Furundarena, L. Meabe, J.M. López del Amo, I.E. Gunathilaka, M. Forsyth, J. Schuhmacher, A. Roters, S. Krachkovskiy, A. Guerfi, M. Armand, M. Martinez-Ibañez, Transport properties and local ions dynamics in LATP-based hybrid solid electrolytes, Small 20 (2024) 2305769. https://doi.org/10.1002/smll.202305769.